Desalination and Water Treatment
www.deswater.com

doi: 10.5004/dwt.2019.24942

172 (2019) 96–105
December

Synthesis of cobalt ferrite nanoparticles via chemical precipitation as an effective photocatalyst for photo Fenton-like degradation of methylene blue

Deniz Uzunoğlu*, Memduha Ergüt, Pınar Karacabey, Ayla Özer

Chemical Engineering Department, Mersin University, Çiftlikköy Campus, Mersin, Turkey, email: denizuzunoglu4@gmail.com (D. Uzunoğlu)

Received 17 May 2019; Accepted 22 September 2019

ABSTRACT

In this work, the synthesis and characterization of cobalt ferrite nanoparticles ($CoFe_2O_4$ NPs) were carried out. The characterization studies confirmed that the synthesized particles were determined to be magnetic $CoFe_2O_4$ NPs in nanoscale and cubic spinel structure. The Brunauer–Emmett–Teller specific surface area of mesoporous $CoFe_2O_4$ NPs was determined to be 145.03 m^2/g. The photo Fenton-like degradation ability of $CoFe_2O_4$ NPs was also evaluated and the results demonstrated that the synergistic effect of combining of Co and Fe_2O_4 enabled $CoFe_2O_4$ NPs to become the promising photo Fenton-like catalyst for degradation of methylene blue (MB) from aqueous solutions. At the optimum experimental conditions (3.0 of initial pH, 25 mM of H_2O_2 concentration, 50 mg/L of initial dye concentration, and 0.25 g/L of catalyst concentration), 18.29% chemical oxygen demand removal and 99.75% color removal were achieved after the photo Fenton-like degradation of MB in the presence of $CoFe_2O_4$ NPs heterogeneous catalyst with near-UV radiation.

Keywords: Cobalt ferrite nanoparticles; Fenton-like; Heterogeneous catalyst; Methylene blue; Photo degradation

1. Introduction

Approximately 7×10^5 tons dye (with more than 10,000 types) per a year are consumed in order to color various materials such as cotton, wool, silk, nylon, polyester, acrylic fiber, paper, leather products, inks, printer cartridge, food products, cosmetics, plastics, gasoline, lubricants, oils, waxes, wood, soaps, detergents, fibers, oils, paints, and plastics in the various industrial areas. Therefore, dye-laden wastewaters pollute natural waters and lower their value in use. In recent years, several techniques have been developed for the treatment of wastewater containing dyes and other contaminants. These techniques can be classified as preliminary, primary, secondary, and tertiary or advanced wastewater treatment. The basic properties of them were summarized in Table 1 [1]. In recent years, advanced oxidation processes such as Fenton, photo-Fenton, sono-Fenton processes, ozonation, electrochemical oxidation, photolysis with H_2O_2, and O_3 electro-Fenton, which are based on the production and the oxidative action of hydroxyl radicals, have attracted great attention for the treatment of a wide range of organic pollutants in wastewaters. The photo Fenton-like (UV/H_2O_2) process could be used promptly as a hopeful and attractive treatment method for an effective decolorization and degradation of dyes in the textile wastewater.

Various heterogeneous nano-based materials such as Fe_3O_4 nanoparticles grown on cellulose/graphene oxide hydrogels [2], Ni-doped Fe_3O_4 nanoparticles coupled with SnS_2 nanosheets [3], graphene-wrapped zero-valent copper nanoparticles [4], CuO nanoparticles [5], $CoFe_2O_4$-reduced graphene oxide [6], $NiFe_2O_4$ nanoparticles [7], Co-doped $MgFe_2O_4$ nanoparticles [8], carbon/$CoFe_2O_4$ nanocomposite [9], Fe-doped CeO_2 nanosheets [10], have already been successfully fabricated and used efficiently for the wastewater treatment. Recently, using spinel ferrite (MFe_2O_4) magnetic

* Corresponding author.

Presented at the 4th International Conference on Recycling and Reuse 2018 (R&R2018), 24–26 October 2018, Istanbul, Turkey

Table 1
Wastewater treatment methods' properties

Method	Purpose
Preliminary treatment methods	Removal of rags, grits, papers, clarification, coarse screening, and comminution of large solids as well as the removal of oil and grease which prevent effective treatment and also diminish the biological oxygen demand of the wastewater.
Primary treatment methods	Elimination of settleable organic and inorganic materials by sedimentation and the exclusion of solid that will froth by skimming.
Secondary treatment methods	Elimination of biodegradable dissolved and colloidal organic matter using aerobic treatment (such as activated sludge, constructed wetland, membrane bioreactor, aerobic/anaerobic bioreactor, trickling filter, rotating biological contactors, facultative lagoons, and bio-oxidation process).
Advanced treatment methods	Removal contaminants with physical techniques (coagulation-flocculation, reverse osmosis, ultrafiltration, microfiltration, nanofiltration, adsorption, chemical techniques (such as ion exchange, chemical precipitation, Fenton/photo-Fenton/electro-Fenton oxidation, electrochemical oxidation, ozonation, photolysis, photocatalysis, solar-driven, ultrasound process), and/or biological techniques (microbial degradation).

nanocomposites as a heterogeneous catalyst, especially in wastewater treatment applications, has gained much attention owing to their distinctive magnetic assets and chemical stability. Moreover, it is easy to remove spinel ferrites magnetic nanocomposites from the treated waste by applying external magnet and recycled. Among them, cobalt ferrite magnetic nanoparticles ($CoFe_2O_4$ NPs) are indispensable metal oxide and they have exclusive applications in various fields like a sensor, semiconductor photocatalysts, biomedical, etc. It is an *n*-type semiconductor, highly stable, small optical band gaps (2.0 eV) making them active under visible light treatment [11]. Therefore, in the present study, cobalt ferrite magnetic nanoparticles ($CoFe_2O_4$ NPs) were synthesized, characterized, and used as a heterogeneous catalyst to investigate the possibility of decolorization of methylene blue (MB) dye by photo Fenton-like process.

2. Materials and methods

2.1. Chemicals

The chemicals $Fe(NO_3)_3{\cdot}6H_2O$ (Acros, Belgium), $Co(NO_3)_2{\cdot}4H_2O$ (Acros, Belgium), NaOH (Merck, North America), H_2O_2 (34.5–36 w/w%, Merck, North America), MB (≥99.0 w/w%, Merck, North America), were analytical grade and purchased commercially. All the chemicals were used directly without any purification method.

2.2. Synthesis and characterization of cobalt ferrite nanoparticles

$CoFe_2O_4$ nanoparticles have been synthesized by chemical precipitation method. The essential mass of ferric nitrate ($Fe(NO_3)_3{\cdot}6H_2O$) and cobalt nitrate ($Co(NO_3)_2{\cdot}4H_2O$) was taken in a stoichiometric ratio of 2:1 and dissolved in distilled water. Then, 1 M of NaOH aqueous solution was added as a reductant to adjust the pH 10, then the formed solution was kept at an ambient temperature of 80°C for 3 h to obtain a thick precipitate. The obtained product was centrifuged using double distilled water and then dried in a hot air oven at 80°C for 24 h. The dried product was powdered well by a mortar and calcined at 500°C for 3 h in a furnace. As a result, $CoFe_2O_4$ nanoparticles ($CoFe_2O_4$ NPs) were obtained [12] and then the obtained $CoFe_2O_4$ NPs were characterized with X-ray Diffractometer (XRD-Philips X'Pert, Netherlands) and scanning electron microscopy (SEM-Zeiss Supra 55, Germany). Also, nitrogen adsorption–desorption measurements were performed by Micromeritics Tristar Orion II 3020 surface area and porosimetry analyzer to determine Brunauer–Emmett–Teller (BET) specific surface area and porosity.

2.3. Photo Fenton-like degradation experiments

Photo Fenton-like activity of $CoFe_2O_4$ nanoparticles was examined by evaluating the degradation of organic MB dye in the presence of aqueous solution under irradiation of visible light with a high-pressure mercury lamp (165 W). In the photo Fenton-like experiments, the desired amount of $CoFe_2O_4$ NPs was added to solutions containing 50 mL of MB solution at known initial pH and initial dye concentrations. Prior to irradiating, the flasks containing the solutions were agitated in the water bath in dark for 20 min to make certain desorption–adsorption equilibrium of MB aqueous solution with the nanocatalyst. Then the aqueous solution with the catalyst was exposed to light after the addition of 5 ml of H_2O_2 solutions. The samples were taken at pre-determined time intervals and the nanoparticles were removed by an external magnet. The concentration of MB was observed with the ultraviolet-visible (UV-vis) spectrophotometer at the wavelength of 665 nm. The decolorization percentage for MB was expressed in terms of the decrease in UV-vis absorbance. The results were reported as the average of three experiments.

3. Results and discussion

3.1. Characterization studies

The structure and phase purity of $CoFe_2O_4$ NPs was confirmed by XRD analysis. The obtained XRD pattern of $CoFe_2O_4$ NPs is given in Fig. 1. Accordingly, the diffraction

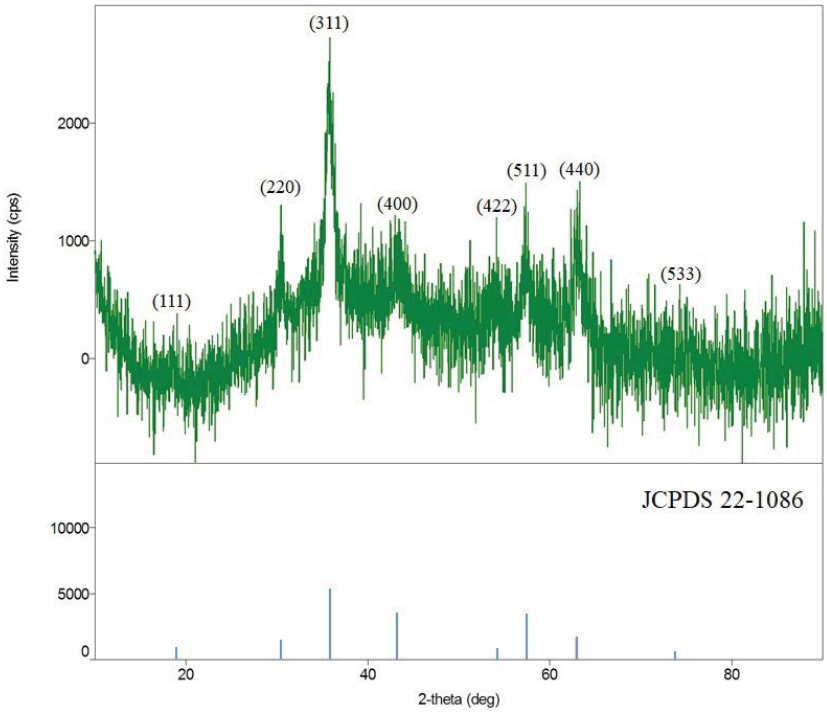

Fig. 1. XRD pattern of $CoFe_2O_4$ NPs.

peaks best fitted to the standard pattern of monophasic cubic $CoFe_2O_4$ with a spinel structure (JCPDS 22-1086). The peaks observed at 18.30°, 30.44°, 35.83°, 43.16°, 53.70°, 57.50°, 62.94°, and 74.90° 2θ can be assigned to (111), (220), (311), (400), (422), (511), (440) and (533) planes of spinel $CoFe_2O_4$, respectively [13]. In the literature, $CoFe_2O_4$ NPs synthesized by polyethylene glycol-assisted hydrothermal method [14], facile hydrothermal method [15], modified solvothermal method [11], one-pot hydrothermal method [16], co-precipitation method [17–23] have the same planes related to the standard pattern of cubic spinel $CoFe_2O_4$ structure.

The crystallite size (D) of $CoFe_2O_4$ NPs was calculated from the most intense peak (311) by using the following Debye–Scherrer's equation [11]:

$$D = \frac{K\lambda}{\beta\cos\theta} \quad (1)$$

where D is the size of crystallite (nm), K is the Scherrer constant, λ is the wavelength of X-ray (CuK_α = 0.154 nm), β is the full width at half maximum of prominent intense peak (rad), and θ is the Bragg's diffraction angle (rad). By using Eq. (1), the crystallite size of the synthesized $CoFe_2O_4$ NPs was calculated as 5.84 nm.

Fig. 2. Magnetic behavior of $CoFe_2O_4$ NPs.

Fig. 2 shows that $CoFe_2O_4$ NPs could be attracted by an external magnet rapidly, which demonstrated that $CoFe_2O_4$ NPs had magnetic properties. When the magnet was removed, $CoFe_2O_4$ NPs were dispersed readily by shaking. This property of $CoFe_2O_4$ NPs provides the easy separation of the catalyst from the aqueous solution.

The morphology of $CoFe_2O_4$ NPs was investigated by SEM analysis given in Figs. 3a–d. The average diameter of $CoFe_2O_4$ NPs was determined to be 35.75 nm before the treatment (Fig. 3b). This value was higher than the value calculated by Debye–Scherrer's equation. The reason for this was considered that the sizes of the agglomerated nanoparticles were measured in the SEM images. Moreover, the synthesized $CoFe_2O_4$ NPs had a sphere-like structure. After treatment, the structure of $CoFe_2O_4$ NPs did not change, which enables the re-use of the catalyst.

To investigate the surface textural property of the adsorbent, N_2 adsorption–desorption measurement was conducted. The BET specific surface area (S_{BET}) of $CoFe_2O_4$ NPs was determined as 145.03 m^2/g. The obtained BET isotherm and Horvath–Kawazoe (HK) pore size distribution (inset) for $CoFe_2O_4$ NPs are presented in Fig. 4. Fig. 4 shows

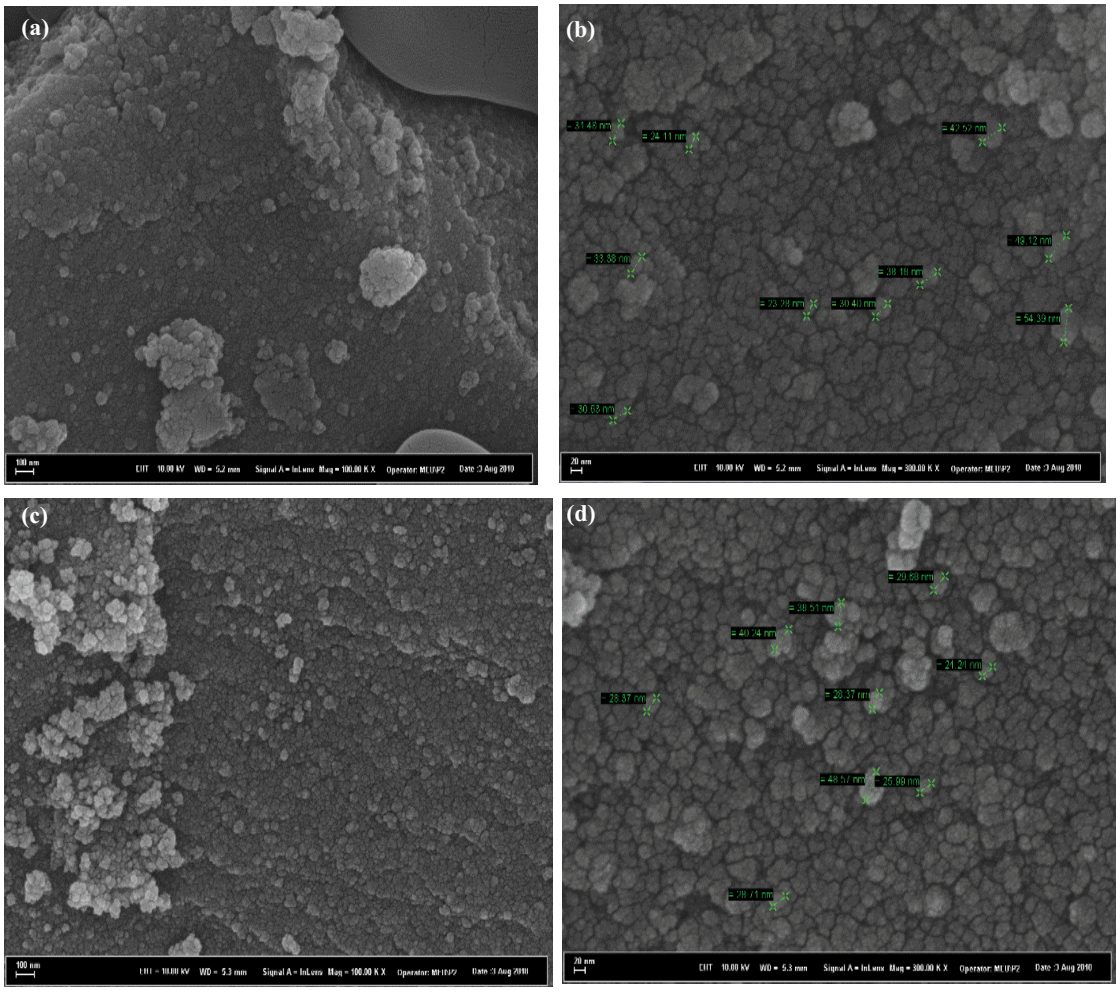

Fig. 3. SEM images of $CoFe_2O_4$ NPs at different magnification (a,b) before and (c,d) after Fenton-like degradation of MB.

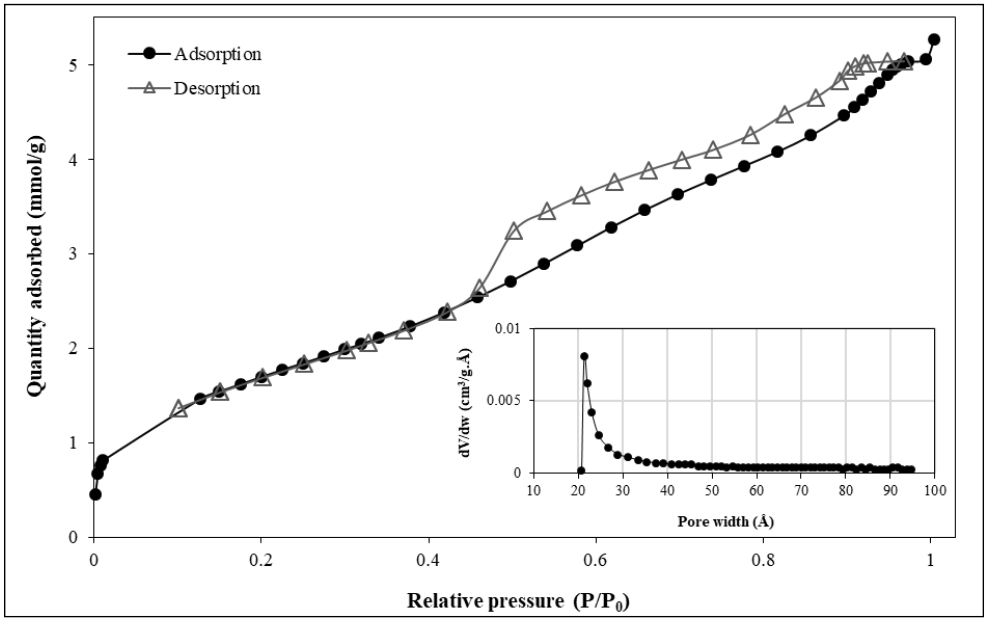

Fig. 4. BET isotherm and pore size distribution (inset) of $CoFe_2O_4$ NPs.

a type IV isotherm (type H_2 hysteresis loop according to International Union of Pure and Applied Chemistry (IUPAC) classification) with an inflection of nitrogen adsorbed volume at P/P_0 about 1.0 which confirmed the formation of mesoporous (2–50 nm) [14]. Barrett–Joyner–Halenda adsorption average pore width of 2.08 nm with 0.044 cm^3/g pore volume confirmed the BET results. According to the pore-size distribution plot in the inset of Fig. 4 obtained by HK method, the sphere-like pores were mainly located in the narrow range of 2.0–3.0 nm, and a peak was seen at 2.12 nm, which indicated the presence of mesopores (2–50 nm). A literature survey for the S_{BET} of various $CoFe_2O_4$ NPs was done and the results are summarized in Table 2. Accordingly, the high S_{BET} makes $CoFe_2O_4$ NPs an efficient candidate as a heterogeneous catalyst for the wastewater treatment processes.

3.2. Color removal studies

The color removal of MB was investigated for different treatment processes and the obtained color removal percentages are presented in Table 3. It is known that H_2O_2 is decomposed into •OH radicals in Fenton like degradation processes. The color removal studies showed that the decomposition of H_2O_2 did not take place under UV light in this work (H_2O_2/UV). Furthermore, $CoFe_2O_4$ NPs could decompose very little of H_2O_2 in the dark ($CoFe_2O_4$ NPs/H_2O_2) and UV irradiation significantly enhanced H_2O_2 decomposition efficiency ($CoFe_2O_4$ NPs/H_2O_2/UV). Moreover, $CoFe_2O_4$ NPs exhibited very poor photocatalytic activity ($CoFe_2O_4$ NPs/UV) whilst nearly 100% photo Fenton-like degradation could be achieved by $CoFe_2O_4$ NPs. However, it was seen that Fe_2O_4 NPs did not have photo Fenton-like catalytic activity (Fe_2O_4 NPs/H_2O_2/UV), and so; it could be concluded that the addition of cobalt to Fe_2O_4 NPs improve the photo Fenton-like catalytic activity. In these regards, the purposed degradation mechanisms were given as follows [31,32]:

$$CoFe_2O_4 + hv \rightarrow CoFe_2O_4\ (h^+ + e^-) \quad (2)$$

$$CoFe_2O_4\ (e^-) + H_2O_2 \rightarrow CoFe_2O_4 + OH^- + {}^\bullet OH \quad (3)$$

$$CoFe_2O_4\ (h^+) + OH^- \rightarrow CoFe_2O_4 + {}^\bullet OH \quad (4)$$

$$MB + {}^\bullet OH \rightarrow \text{degradation products} \quad (5)$$

Accordingly, hole/electron (h^+/e^-) pairs were firstly photogenerated on the catalyst under UV irradiation (Eq. (2)). Then, electrons on $CoFe_2O_4$ NPs were reacted with H_2O_2 to produce both OH^- ions and •OH radicals (Eq. (3)). At the same time, photogenerated holes (h^+) reacted with OH^- to yield •OH radicals (Eq. (4)). In this way, the generated •OH radicals attacked the dye molecules, resulting in the degradation of them (Eq. (5)). The photo Fenton-like degradation of MB by $CoFe_2O_4$ NPs was also evaluated by recording the UV-vis spectra of dye solution by time (Fig. 5).

As shown in Fig. 5, the maximum absorption peaks were observed in the range of 575–675 nm, which was assigned to π-π* transition of –N=N– (azo) bond. The intensity of peak decreased by time depending on the breakage of the –N=N– bond, resulting in the vanishing of the blue color of MB.

Table 2
BET specific surface area of various $CoFe_2O_4$ nanoparticles in the literature

Material	BET specific surface area (S_{BET}, m^2/g)	References
$CoFe_2O_4$ ferrite nanoparticles	173.00	[24]
$CoFe_2O_4$ nanoparticles	145.03	This study
$CoFe_2O_4$ nanoparticles	140.90	[25]
Mesoporous $CoFe_2O_4$ nanoparticles	140.60	[26]
Magnetic $CoFe_2O_4$ nanoparticles	103.48	[27]
Mesoporous $CoFe_2O_4$ nanospheres	85.40	[15]
$CoFe_2O_4$ nanoparticles	82.80	[14]
$CoFe_2O_4$ magnetic nanoparticles	76.00	[11]
$CoFe_2O_4$ nanoparticles	73.97	[28]
$CoFe_2O_4$ nanoparticles	49.77	[29]
$CoFe_2O_4$ nanoparticles	48.14	[30]
$CoFe_2O_4$ nanoparticles	15.24	[16]

Table 3
MB color removal percentages for different treatment processes (experimental conditions: (1) C_0 = 50 mg/L, pH = 3.0, T = 25°C, 25 mM H_2O_2, t = 300 min, (2) C_0 = 50 mg/L, pH = 3.0, T = 25°C, X_0 = 0.25 g/L, and (3)–(5) C_0 = 50 mg/L, pH = 3.0, T = 25°C, X_0 = 0.25 g/L, 25 mM H_2O_2)

Process	Color removal %
(1) H_2O_2/UV	0.85
(2) $CoFe_2O_4$ NPs/UV	1.65
(3) $CoFe_2O_4$ NPs/H_2O_2	4.84
(4) $CoFe_2O_4$ NPs/H_2O_2/UV	99.99
(5) Fe_2O_4 NPs/H_2O_2/UV	2.18

However, any new peak formation was not observed in the spectra. Furthermore, two bands in the ultraviolet region located at the ranges of 275–300 nm and 250–275 nm were associated with benzene and naphthalene structures in MB, respectively. The intensities of these bands also decreased by time because of aromatic fragmentation in the dye molecule and its intermediates [33].

As a result, the synthesized $CoFe_2O_4$ NPs were evaluated as heterogeneous photo Fenton-like catalyst in the degradation of MB because the highest color removal percentage was achieved by this process. Therefore, the effects of various environmental conditions on the photo Fenton-like reaction were investigated. The obtained results were given as follows.

3.2.1. Effect of initial pH

The effect of initial pH on the degradation of MB in presence of $CoFe_2O_4$ NPs was investigated in the initial pH range of 3.0–5.0 at H_2O_2 concentration of 25 mM, the initial MB concentration of 50 mg/L, the temperature of 25°C, and the catalyst concentration of X_0 = 0.25 g/L. The color removal percentages at the end of 300 min are presented in Fig. 6a.

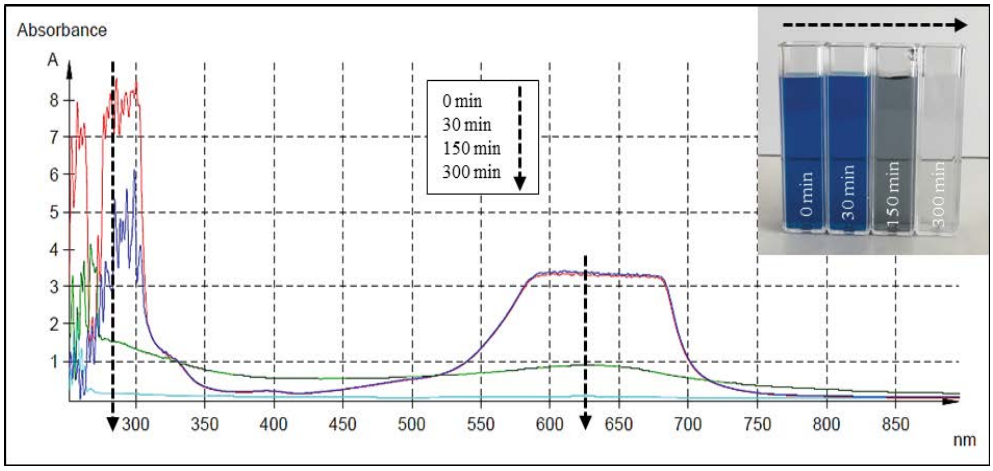

Fig. 5. UV-vis spectra of dye solution by the time.

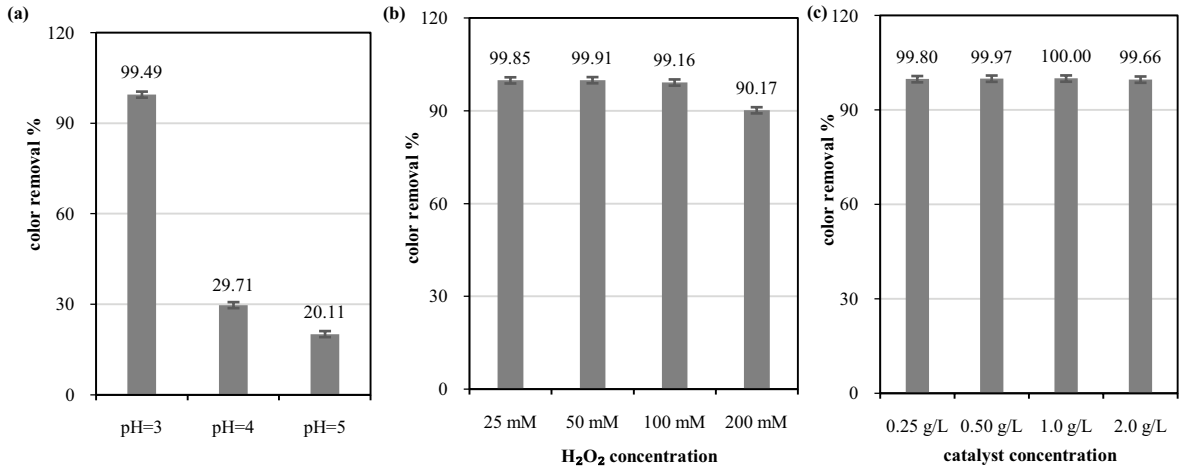

Fig. 6. (a) Effect of initial pH (25 mM H_2O_2, C_0 = 50 mg/L, T = 25°C, X_0 = 0.25 g/L), (b) effect of H_2O_2 concentration (pH = 3.0, C_0 = 50 mg/L, T = 25°C, X_0 = 0.25 g/L), and (c) effect of catalyst concentration (pH = 3.0, 25 mM H_2O_2, C_0 = 50 mg/L, T = 25°C).

As shown in Fig. 6a, 99.49 % color removal could be achieved at the initial pH = 3.0 whilst as the initial pH increased from 4.0 to 5.0, the color removal percentage decreased from 29.71% to 20.11%. This case could be explained based on the following three factors [34]:

- The oxidation potential of •OH radicals increases with the decrease in initial pH; and thus, the color removal percentages may reduce by increasing in initial pH.
- At high initial pH values, H_2O_2 decomposes to O_2 and H_2O; and thus lower •OH radicals form during the reaction. As a result of it, color removal percentages may decrease.
- More •OH radicals are produced at the strongly acidic medium depending on the dissolving of more iron ions, and thus color removal percentages may increase.

Consequently, the optimum initial pH was determined to be 3.0. Similarly to this work, the various studies about photo Fenton-like degradation of the contaminants in the literature have indicated that the strong acidic conditions enhance the formation of radicals and the oxidation of contaminants [35–37].

3.2.2. *Effect of H_2O_2 concentration*

Evaluating of H_2O_2 concentration is important because the major cost associated with such processes is H_2O_2 concentration. In this study, the effect of H_2O_2 concentration on the degradation of MB in the presence of $CoFe_2O_4$ NPs was investigated in the H_2O_2 concentration range of 25–200 mM at the initial pH of 3.0, the initial MB concentration of 50 mg/L, the temperature of 25°C, and the catalyst concentration of X_0 = 0.25 g/L. The color removal percentages at the end of 300 min are presented in Fig. 6b. Accordingly, nearly the same color removal percentage (≈99%) was obtained in the range of 25–100 mM, and it decreased from 99% to 90% thereafter. It is well-known that at high H_2O_2 concentration, that is, beyond 100 mM for this work, scavenging of •OH radicals take place with the increase in H_2O_2 concentration generating

perhydroxyl radicals ($HO_2^{\bullet}$), which is less strong oxidant as compared to $^{\bullet}OH$ radicals ($H_2O_2 + {}^{\bullet}OH \rightarrow H_2O + HO_2^{\bullet}$). At the same time, the formed $HO_2^{\bullet}$ could further consume the $^{\bullet}OH$ radicals ($HO_2^{\bullet} + {}^{\bullet}OH \rightarrow H_2O + O_2$) [38]. As a result of this effect, the color removal percentage reduced when H_2O_2 concentration was increased beyond 100 mM. Therefore, take into account the process cost and the environmental reasons; the optimum H_2O_2 concentration was chosen as 25 mM. Similar to the scavenging effect of $OH^{\bullet}$ radical has been observed in the various studies about photo Fenton-like degradation of MB in the literature [39–42]. Accordingly, the color removal percentages decreased at the higher H_2O_2 concentrations because there were more $HO_2^{\bullet}$ radicals, formed at the end of the reaction of the scavenging effect of $OH^{\bullet}$, in the medium.

3.2.3. Effect of catalyst concentration

The effect of catalyst concentration on the degradation of MB in presence of $CoFe_2O_4$ NPs was investigated in the catalyst concentration range of 0.25–2.0 g/L at initial pH of 3.0, the initial MB concentration of 50 mg/L, the temperature of 25°C, and H_2O_2 concentration of 25 mM. The color removal percentages at the end of 300 min are presented in Fig. 6c. As shown in Fig. 6c, almost 100% of the color removal percentages were obtained in the studied catalyst concentration range. It was concluded that the catalyst concentration had an insignificant effect on the degradation process. Therefore, take into account the process cost; the optimum catalyst concentration was obtained as 0.25 g/L.

3.2.4. Effect of contact time and initial dye concentration

The effect of contact time on the degradation of MB in presence of $CoFe_2O_4$ NPs was investigated for different initial dye concentrations at an initial pH of 3.0, the temperature of 25°C, and H_2O_2 concentration of 25 mM, and the catalyst concentration of X_0 = 0.25 g/L. The obtained color removal percentages at the pre-determined contact time intervals are shown in Fig. 7a. As can be seen in Fig. 7a, for all initial dye concentrations, the color removal percentage was increased up to 300 min, and thereafter it remained nearly constant.

The effect of initial dye concentration was also evaluated and the color removal percentages at the end of 300 min were given in the bar chart (Fig. 7b). Accordingly, the color removal percentage reduced gradually by increasing initial dye concentration. This case could be ascribed based on the following four factors [6,43]:

- As the initial dye concentration increases, the adsorption of dye molecules on the surface of the catalyst also increases; and this case prevents the catalyst to absorb the energy. For this reason, lower $^{\bullet}OH$ radicals are generated and thus, the color removal percentages may decrease.
- The higher adsorption of dye molecules on the surface of the catalyst may block the active sites on the surface of the catalyst, causing the lower generation of $^{\bullet}OH$ radicals and thus, the color removal percentages may decrease.
- When there are more dye molecules in the reaction medium, they compete against the intermediates produced during the reaction and thus, the color removal percentages may decrease.
- At the higher initial dye concentration, the photons are blocked before reaching the surface of the catalyst, which may cause a decrease in the color removal percentages.

As a result of the similar factors, the initial dye concentration has a negative effect on the photo Fenton-like degradation of various model pollutants [44–46].

In spite of these factors, 60.97% removal percentage could be achieved with 0.25 g/L of $CoFe_2O_4$ NPs even at a high initial dye concentration of 500 mg/L in this study. This indicated that the synthesized $CoFe_2O_4$ NPs heterogeneous catalyst could be suggested for an industrial application about the treatment of wastewaters containing high-concentration dye.

According to the obtained results, the optimum initial pH, H_2O_2 concentration, initial dye concentration, and catalyst concentration was determined to be 3.0, 25 mM, 50 mg/L, and 0.25 g/L.

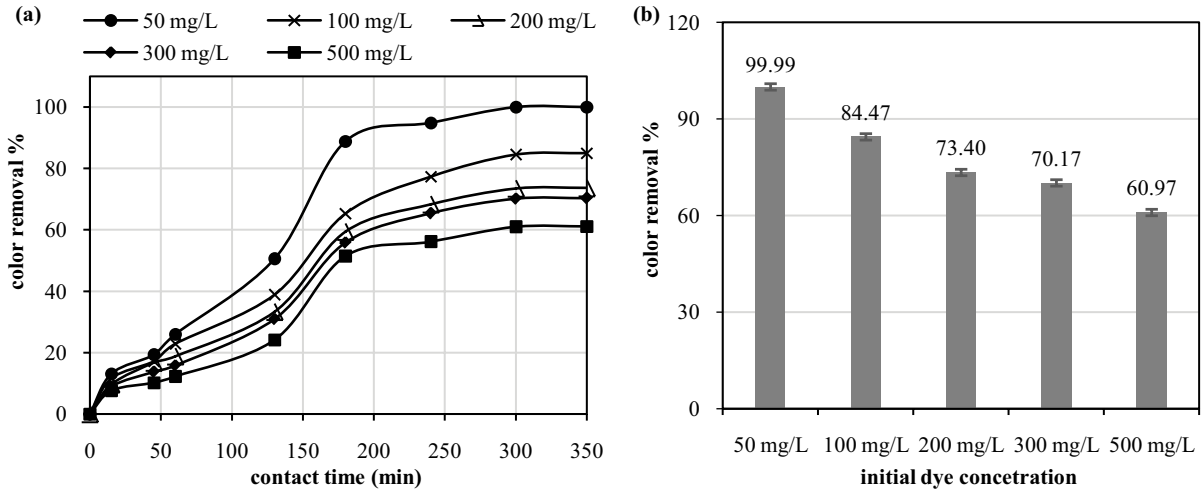

Fig. 7. Effect of (a) contact time and (b) initial dye concentration (pH = 3.0, 25 mM H_2O_2, T = 25°C, X_0 = 0.25 g/L).

3.2.5. Chemical oxygen demand removal

Chemical oxygen demand (COD) demonstrates the concentration of organic compounds present in the wastewater and its measurement reflects the total quantity of oxygen required for oxidation of organics into carbon dioxide and water. In this study, COD removal at the obtained optimum environmental conditions was evaluated and the results showed that 18.29% COD removal and 99.75% color removal were achieved at these conditions. The color removal result indicated the almost destruction of the chromophore group of MB while the COD removal showed the partial oxidation of the organic pollutants to CO_2 and H_2O. Consequently, it could be said that MB transformed into colorless intermediates at the end of the treatment process and these intermediates gave rise to the COD value.

A literature survey has been done for photo Fenton-like degradation of MB with various catalysts, and the literature summary is presented in Table 4.

The literature survey showed that it has been studied at low initial dye concentrations in the other works in the literature. However, in this study, it was tried to study at high initial dye concentration, and relatively high color removal percentage was achieved even at high initial dye concentration. Besides, the optimum catalyst concentration in this study was generally lower than the other studies in the literature. The possibility to study at high dye concentrations and low catalyst concentrations are the most important advantages for industrial applications. On the other hand, unlike this study, the catalysts used in the literature have been generally combined with the support materials, which increases the process cost. Although any support material was not used for the catalyst in this study, as high color removal capacity as in the other studies could be achieved. This situation may have only caused a prolongation of the reaction time, which may be a disadvantage in terms of the process cost. The results proved that the photo Fenton-like process using magnetic $CoFe_2O_4$ NPs would be a highly efficient and cost-effective solution to decolor of MB at even high dye concentration and low catalyst concentration. Moreover, there were several studies about the photo Fenton-like degradation of MB with various catalysts; however, it was found only two studies about the photo Fenton-like degradation of MB with $CoFe_2O_4$ NPs [12,47], and the effects of environmental conditions on the process have not been investigated in details in these studies. The present work has focused on both the characterization of the catalyst and the investigation of the photo Fenton-like degradation process in detail.

Consequently, differently from the other studies, a heterogeneous photo Fenton-like magnetic nanocatalyst has been synthesized via a simple and cheap method by not using any supporting material and harmful solvents; and then, the as-synthesized catalyst could be utilized efficiently in the photo Fenton-like degradation of MB even at low catalyst concentration and high initial dye concentration. Besides, COD removal, which is an important factor for the industrial applications, has not been investigated for the photo Fenton-like degradation of MB with various catalysts given in Table 4. In this regard, another important contribution of this work for the related literature is that $CoFe_2O_4$ NPs have the capacity of 18.29% COD removal as well as 99.75%

Table 4
Color removal percentages along with the experimental conditions for photo Fenton-like degradation of MB with various catalyst

Catalyst	C_0 (mg/L)	Color removal (%)	T (°C)	pH	$C_{H_2O_2}$ (mM)	Reaction time (min)	X_0 (g/L)	Light source	References
$CoFe_2O_4$ NPs	50	99.75	25	3.0	25	300	0.25	High-pressure mercury lamp (165 W)	This study
	500	60.97							
$CoFe_2O_4$ NPs	20	99.30	–	9.0	Concentrated	75	1.0	High-pressure mercury lamp (125 W)	[12]
$CoFe_2O_4$ NPs	10	99.80	–	–	–	100	1.0	Visible light	[47]
V-Ti co-doped magnetite	64	96	25	7.0	10	120	1.0	UV light (6 W)	[48]
RGO/Fe_3O_4	20	96	25	6.0	10	120	0.25	Xenon lamp (300 W)	[49]
α-Fe_2O_3@GO	40	96	20	3.0	1.1	80	0.25	High-pressure mercury lamp (100 W)	[50]
Magnetite	16	88.85	25	4.0	–	30	2.5	UV lamp	[51]
CdS/MWCNT-TiO_2	16	98	20	3.5	0.6	30	0.75	White fluorescent lamp (8 W)	[52]
Fe–Ni/SiO_2	20	99.80	30	3.0	3.0	60	0.85	Xenon lamp (500 W)	[39]
FePcS-LDH	10	99.80	25	6.0	10.30	180	0.01	Xenon lamp (400 W)	[40]
Tris(1,10)-phenanthroline iron(II) loaded on zeolite	11.5	92.6	25	6.5	6.6	140	10	UV-vis lamp (300 W)	[41]
LiFe$(WO_4)_2$	100	94	25	3.0–9.0	10	60	1.0	UV lamp (20 W)	[42]

color removal for the photo Fenton-like degradation of MB at mild conditions.

4. Conclusions

In this study, $CoFe_2O_4$ NPs were synthesized successfully with outstanding properties such as strong magnetism, mesoporosity, high surface area, homogenous sphere-like structure. The characterization studies showed the following finding; the synthesized material was found as the monophasic cubic $CoFe_2O_4$ with a spinel structure with XRD analysis, SEM analysis indicated that the synthesized $CoFe_2O_4$ NPs had sphere-like structure, the BET specific surface area of $CoFe_2O_4$ NPs was determined as 145.03 m^2/g. Then, the degradation of MB could be achieved in presence of near-UV light when both oxidant (H_2O_2) and the synthesized $CoFe_2O_4$ NPs were present together in the reaction medium, thus proving that the dye was decolorized by photo Fenton-like reaction. The effects of various environmental conditions on the photo Fenton-like degradation of MB with $CoFe_2O_4$ NPs were also investigated. According to the obtained results; the optimum initial pH, H_2O_2 concentration, initial dye concentration, and catalyst concentration for photo Fenton-like degradation of MB with $CoFe_2O_4$ NPs were determined to be 3.0, 25 mM, 50 mg/L, and 0.25 g/L, respectively. At these optimum conditions, 18.29% COD removal and 99.75% color removal were obtained. The obtained results and the literature survey indicated that $CoFe_2O_4$ NPs is a promising heterogeneous photo Fenton-like magnetic nanocatalyst for the degradation of MB. On the other hand, it could be suggested that $CoFe_2O_4$ NPs can be combined with various materials to increase COD removal. After this aim has been achieved, the treatment process can be scaled up for the practical application, and the high color and COD removal can be achieved in this way. Also, the synthesized $CoFe_2O_4$ NPs could be utilized as a heterogeneous photo Fenton-like magnetic catalyst for the different organic pollutants.

Consequently, the present study has revealed significant outputs to the synthesis and characterization of an effective photo Fenton-like heterogeneous nanocatalyst, which could be important for the contribution to the related literature as well as the water treatment applications.

References

[1] A. Nasar, F. Mashkoor, Application of polyaniline-based adsorbents for dye removal from water and wastewater—a review, Environ. Sci. Pollut. Res., 26 (2019) 5333–5356.

[2] Y. Chen, P. Pötschke, J. Pionteck, B. Voit, H.S. Qi, Fe_3O_4 nanoparticles grown on cellulose/GO hydrogels as advanced catalytic materials for the heterogeneous fenton-like reaction, ACS Omega, 4 (2019) 5117–5125.

[3] A.L. Zhang, L.Y. Zhu, Z.D. Nan, Ni-doped Fe_3O_4 nanoparticles coupled with SnS_2 nanosheets as 0D/2D heterogeneous catalyst for photo-Fenton reaction, Mater. Chem. Phys., 224 (2019) 156–168.

[4] L.J. Xu, Y.J. Yang, W.Y. Li, Y.J. Tao, Z.G. Sui, S. Song, J. Yang, Three-dimensional macroporous graphene-wrapped zero-valent copper nanoparticles as efficient micro-electrolysis-promoted Fenton-like catalysts for metronidazole removal, Sci. Total Environ., 658 (2019) 219–233.

[5] L. Wang, J.J. Hou, S.Z. Liu, A.J. Carrier, T. Guo, Q.S. Liang, D. Oakley, X. Zhang, CuO nanoparticles as haloperoxidase-mimics: chloride-accelerated heterogeneous Cu-Fenton chemistry for H_2O_2 and glucose sensing, Sens. Actuators, B, 287 (2019) 180–184.

[6] A. Hassani, G. Çelikdağ, P. Eghbali, M. Sevim, S. Karaca, Ö. Metin, Heterogeneous sono-Fenton-like process using magnetic cobalt ferrite-reduced graphene oxide ($CoFe_2O_4$-rGO) nanocomposite for the removal of organic dyes from aqueous solution, Ultrason. Sonochem., 40 (2018) 841–852.

[7] J.F. Qu, T.H. Che, L.B. Shi, Q.H. Lu, S.T. Qi, A novel magnetic silica supported spinel ferrites $NiFe_2O_4$ catalyst for heterogeneous Fenton-like oxidation of rhodamine B, Chin. Chem. Lett., 30 (2019) 1198–1203.

[8] Y.F. Diao, Z.K. Yan, M. Guo, X.D. Wang, Magnetic multi-metal co-doped magnesium ferrite nanoparticles: an efficient visible light-assisted heterogeneous Fenton-like catalyst synthesized from saprolite laterite ore, J. Hazard. Mater., 344 (2018) 829–838.

[9] M.R. Heidari, R.S. Varma, M. Ahmadian, M. Pourkhosravani, S.N. Asadzadeh, P. Karimi, M. Khatami, Photo-Fenton like catalyst system: activated Carbon/$CoFe_2O_4$ nanocomposite for reactive dye removal from textile wastewater, Appl. Sci., 9 (2019) 963.

[10] W. Wang, Q. Zhu, F. Qin, Q.G. Dai, X.Y. Wang, Fe doped CeO_2 nanosheets as Fenton-like heterogeneous catalysts for degradation of salicylic acid, Chem. Eng. J., 333 (2018) 226–239.

[11] A. Kalam, A.G. Al-Sehemi, M. Assiri, G. Du, T. Ahmad, I. Ahmad, M. Pannipara, Modified solvothermal synthesis of cobalt ferrite ($CoFe_2O_4$) magnetic nanoparticles photocatalysts for degradation of methylene blue with H_2O_2/visible light, Res. Phys., 8 (2018) 1046–1053.

[12] P.A. Vinosha, S.J. Das, Investigation on the role of pH for the structural, optical and magnetic properties of cobalt ferrite nanoparticles and its effect on the photo-Fenton activity, Mater. Today:. Proc., 5 (2018) 8662–8671.

[13] L.X. Zhang, Y.X. Sun, W.B. Jia, S.S. Ma, B. Song, Y. Li, H.F. Jiu, J.W. Liu, Multiple shell hollow $CoFe_2O_4$ spheres: synthesis, formation mechanism and properties, Ceram. Int., 40 (2014) 8997–9002.

[14] X.F. Wu, W. Wang, F. Li, S. Khaimanov, N. Tsidaeva, M. Lahoubi, PEG-assisted hydrothermal synthesis of $CoFe_2O_4$ nanoparticles with enhanced selective adsorption properties for different dyes, Appl. Surf. Sci., 389 (2016) 1003–1011.

[15] M.P. Reddy, A.M.A. Mohamed, X.B. Zhou, S. Du, Q. Huang, A facile hydrothermal synthesis, characterization and magnetic properties of mesoporous $CoFe_2O_4$ nanospheres, J. Magn. Magn. Mater., 388 (2015) 40–44.

[16] B. Paul, D.D. Purkayastha, S.S. Dhar, One-pot hydrothermal synthesis and characterization of $CoFe_2O_4$ nanoparticles and its application as magnetically recoverable catalyst in oxidation of alcohols by periodic acid, Mater. Chem. Phys., 181 (2016) 99–105.

[17] M. Vadivel, R.R. Babu, K. Sethuraman, K. Ramamurthi, M. Arivanandhan, Synthesis, structural, dielectric, magnetic and optical properties of Cr substituted $CoFe_2O_4$ nanoparticles by co-precipitation method, J. Magn. Magn. Mater., 362 (2014) 122–129.

[18] M. Vadivel, R.R. Babu, K. Ramamurthi, M. Arivanandhan, CTAB cationic surfactant assisted synthesis of $CoFe_2O_4$ magnetic nanoparticles, Ceram. Int., 42 (2016) 19320–19328.

[19] S. Ayyappan, J. Philip, B. Raj, A facile method to control the size and magnetic properties of $CoFe_2O_4$ nanoparticles, Mater. Chem. Phys., 115 (2009) 712–717.

[20] K. Praveena, B. Radhika, S. Srintah, Size effects on structural and magnetic properties of $CoFe_2O_4$ nanoparticles prepared by co-precipitation method, AIP Conf. Proc., 1447 (2012) 289–290.

[21] M. Vadivel, R.R. Babu, K. Ramamurthi, M. Arivanandhan, Effect of PVP concentrations on the structural, morphological, dielectric and magnetic properties of $CoFe_2O_4$ magnetic nanoparticles, Nano-Struct. Nano-Objects, 11 (2017) 112–123.

[22] M. Vadivel, R.R. Babu, M. Arivanandhan, K. Ramamurthi, Y. Hayakawa, Role of SDS surfactant concentrations on the structural, morphological, dielectric and magnetic properties of $CoFe_2O_4$ nanoparticles, RSC Adv., 5 (2015) 27060–27068.

[23] W.Y. Fu, S.K. Liu, W.H. Fan, H.B. Yang, X.F. Pang, J. Xu, G.T. Zou, Hollow glass microspheres coated with $CoFe_2O_4$ and its microwave absorption property, J. Magn. Magn. Mater., 316 (2007) 54–58.
[24] Z. Ding, W. Wang, Y.J. Zhang, F. Li, J.P. Liu, Synthesis, characterization and adsorption capability for Congo red of $CoFe_2O_4$ ferrite nanoparticles, J. Alloys Compd., 640 (2015) 362–370.
[25] J.K. Rajput, G. Kaur, $CoFe_2O_4$ nanoparticles: an efficient heterogeneous magnetically separable catalyst for "click" synthesis of arylidene barbituric acid derivatives at room temperature, Chin. J. Catal., 34 (2013) 1697–1704.
[26] L.L. Lv, Q. Xu, R. Ding, L. Qi, H.Y. Wang, Chemical synthesis of mesoporous $CoFe_2O_4$ nanoparticles as promising bifunctional electrode materials for supercapacitors, Mater. Lett., 111 (2013) 35–38.
[27] H.X. Zhang, H.R. Li, Z.J. Wang, B. Li, X.W. Cheng, Q.F. Cheng, Synthesis of magnetic $CoFe_2O_4$ nanoparticles and their efficient degradation of diclofenac by activating persulfate via formation of sulfate radicals, J. Nanosci. Nanotechnol., 18 (2018) 6942–6948.
[28] R. Qin, F. Li, W. Jiang, L. Liu, Salt-assisted low temperature solid state synthesis of high surface area $CoFe_2O_4$ nanoparticles, J. Mater. Sci. Technol., 25 (2009) 69–72.
[29] Z. Jiao, X. Geng, M.H. Wu, Y. Jiang, B. Zhao, Preparation of $CoFe_2O_4$ nanoparticles by spraying co-precipitation and structure characterization, Colloids Surf., A, 313 (2008) 31–34.
[30] K.K. Senapati, C. Borgohain, P. Phukan, Synthesis of highly stable $CoFe_2O_4$ nanoparticles and their use as magnetically separable catalyst for Knoevenagel reaction in aqueous medium, J. Mol. Catal. A: Chem., 339 (2011) 24–31.
[31] A.A. Al-Kahtani, M.F.A. Taleb, Photocatalytic degradation of Maxilon C.I. basic dye using CS/$CoFe_2O_4$/GONCs as a heterogeneous photo-Fenton catalyst prepared by gamma irradiation, J. Hazard. Mater., 309 (2016) 10–19.
[32] X. Chen, Z. Wu, D. Liu, Z. Gao, Preparation of ZnO photocatalyst for the efficient and rapid photocatalytic degradation of azo dyes, Res. Lett., 12 (2017) 143.
[33] H.Y. Li, Y.L. Li, L.J. Xiang, Q.Q. Huang, J.J. Qiu, H. Zhang, M.V. Sivaiah, F. Baron, J. Barrault, S. Petit, S. Valange, Heterogeneous photo-Fenton decolorization of Orange II over Al-pillared Fe-smectite: response surface approach, degradation pathway, and toxicity evaluation, J. Hazard. Mater., 287 (2015) 32–41.
[34] A. Khataee, P. Gholami, B. Vahid, Catalytic performance of hematite nanostructures prepared by N_2 glow discharge plasma in heterogeneous Fenton-like process for acid red 17 degradation, J. Ind. Eng. Chem., 50 (2017) 86–95.
[35] F.F. Dias, A.A.S. Oliveira, A.P. Arcanjo, F.C.C. Moura, J.G.A. Pacheco, Residue-based iron catalyst for the degradation of textile dye via heterogeneous photo-Fenton, Appl. Catal., B, 186 (2016) 136–142.
[36] H.C. Lan, A.M. Wang, R.P. Liu, H.J. Liu, J.H. Qu, Heterogeneous photo-Fenton degradation of acid red B over Fe_2O_3 supported on activated carbon fiber, J. Hazard. Mater., 285 (2015) 167–172.
[37] Z. Jia, J. Kang, W.C. Zhang, W.M. Wang, C. Yang, H. Sun, D. Habibi, L.C. Zhang, Surface aging behaviour of Fe-based amorphous alloys as catalysts during heterogeneous photo Fenton-like process for water treatment, Appl. Catal., B, 204 (2017) 537–547.
[38] X.G. Shi, A. Tian, J.H. You, H. Yang, Y.Z. Wang, X.X. Xue, Degradation of organic dyes by a new heterogeneous Fenton reagent-Fe_2GeS_4 nanoparticle, J. Hazard. Mater., 353 (2018) 182–189.
[39] Y. Ahmed, Z. Yaakob, P. Akhtar, Degradation and mineralization of methylene blue using a heterogeneous photo-Fenton catalyst under visible and solar light irradiation, Catal. Sci. Technol., 6 (2016) 1222–1232.
[40] X.X. Tang, Y. Liu, Heterogeneous photo-Fenton degradation of methylene blue under visible irradiation by iron tetrasulphophthalocyanine immobilized layered double hydroxide at circumneutral pH, Dyes Pigm., 134 (2016) 397–408.
[41] J. Zhang, F.-T. Hu, Q.-Q. Liu, X. Zhao, S.-Q. Liu, Application of heterogenous catalyst of tris(1,10)-phenanthroline iron(II) loaded on zeolite for the photo-Fenton degradation of methylene blue, React. Kinet. Mech. Lett., 103 (2011) 299–310.
[42] F. Ji, C.L. Li, J.H. Zhang, L. Deng, Heterogeneous photo-Fenton decolorization of methylene blue over $LiFe(WO_4)_2$ catalyst, J. Hazard. Mater., 186 (2011) 1979–1984.
[43] K. Chanderia, S. Kumar, J. Sharma, R. Ameta, P.B. Punjabi, Degradation of Sunset Yellow FCF using copper loaded bentonite and H_2O_2 as photo-Fenton like reagent, Arabian J. Chem., 10 (2017) S205–S211.
[44] B. Kakavandi, A. Takdastan, S. Pourfadakari, M. Ahmadmoazzam, S. Jorfi, Heterogeneous catalytic degradation of organic compounds using nanoscale zero-valent iron supported on kaolinite: mechanism, kinetic and feasibility studies, J. Taiwan Inst. Chem. Eng., 96 (2019) 329–340.
[45] J. Singh, S. Sharma, Aanchal, S. Basu, Synthesis of Fe_2O_3/TiO_2 monoliths for the enhanced degradation of industrial dye and pesticide via photo-Fenton catalysis, J. Photochem. Photobiol., A, 376 (2019) 32–42.
[46] L.J. Di, H. Yang, T. Xian, X.G. Liu, X.J. Chen, Photocatalytic and photo-Fenton catalytic degradation activities of Z-scheme $Ag_2S/BiFeO_3$ heterojunction composites under visible-light irradiation, Nanomaterials (Basel), 9 (2019) 399.
[47] P.A. Vinosha, L.A. Mely, G.I.N. Mary, K. Mahalakshmi, S.J. Das, Study on cobalt ferrite nanoparticles synthesized by co-precipitation technique for photo-Fenton application, Mech. Mater. Sci. Eng. J., 9 (2017), doi:10.2412/mmse.36.49.466.
[48] X.L. Liang, Y.H. Zhong, S.Y. Zhu, L.Y. Ma, P. Yuan, J.X. Zhu, H.P. He, Z. Jiang, The contribution of vanadium and titanium on improving methylene blue decolorization through heterogeneous UV-Fenton reaction catalyzed by their co-doped magnetite, J. Hazard. Mater., 199 (2012) 247–254.
[49] X.Y. Jiang, L.L. Li, Y.R. Cui, F.L. Cui, New branch on old tree: green-synthesized RGO/Fe_3O_4 composite as a photo-Fenton catalyst for rapid decomposition of methylene blue, Ceram. Int., 43 (2017) 14361–14368.
[50] Y.Y. Liu, W. Jin, Y.P. Zhao, G.S. Zhang, W. Zhang, Enhanced catalytic degradation of methylene blue by α-Fe_2O_3/graphene oxide via heterogeneous photo-Fenton reactions, Appl. Catal., B, 206 (2017) 642–652.
[51] K.M. Reza, A. Kurny, F. Gulshan, Photocatalytic degradation of methylene blue by magnetite+H_2O_2+UV process, J. Environ. Sci. Dev., 7 (2016) 325.
[52] J.R. Kim, E.S. Kan, Heterogeneous photo-Fenton oxidation of methylene blue using CdS-carbon nanotube/TiO_2 under visible light, J. Ind. Eng. Chem., 21 (2015) 644–652.